PCCP

PAPER

View Article Online
View Journal

Cite this: DOI: 10.1039/d6cp00851h

Electronic behavior and structural robustness of recently synthesized CoO_2 nanoscrolls

Guilherme da Silva Lopes Fabris, [a] Ricardo Paupitz, [b] Marcelo L. Pereira Junior [c] and Douglas Soares Galvão *[a]

Received 7th March 2026,
Accepted 5th June 2026

DOI: 10.1039/d6cp00851h

rsc.li/pccp

Cobalt dioxide (CoO_2) is a metastable material in its two-dimensional (2D) form. However, it can be stabilized in the form of nanoscrolls, which have been recently synthesized and shown to display long-term stability and remarkable electronic properties. In this work, we have investigated through Density Functional Tight-Binding simulations their structural and electronic properties. Nanoscrolls with 1.5, 2, and 3 turns were considered, exhibiting increasing stability due to van der Waals interactions. The analysis of the electronic structure confirms the metallic nature of these systems, and the charge density results emphasize the role of oxygen atoms in charge displacement, with the Highest Occupied Crystal Orbital (HOCO) and the Lowest Unoccupied Crystal Orbital (LUCO) spatially localized at opposite edges due to curvature effects. Molecular dynamics simulations demonstrate that the nanoscrolls remain stable up to 600 K. The optimized interlayer distance of 0.46 nm and the slight structural flattening observed in the simulations are both consistent with experimental reports. These results provide a coherent description of the stability, charge distribution, and metallic character of CoO_2 nanoscrolls.

1 Introduction

In recent decades, significant advances have been achieved through research on low-dimensional materials.[1–3] Extensive efforts have been devoted to exploring and tuning the mechanical, electronic, and chemical characteristics of these materials, often by introducing modifications or by synthesizing inorganic analogues of graphene[4]pt such as silicene,[5,6] antimonene,[7,8] hexagonal boron nitride (h-BN),[9] or binary compounds.[10,11] Among these low-dimensional structures, polymers,[12,13] nanoribbons,[14,15] nanotubes,[16,17] and nanoscrolls[18–21] are particularly relevant. Nanoscrolls are formed by the continuous rolling of a monolayer or multiple layers into a spiral form and have been widely investigated in recent years, attracting attention due to their tunable properties and structural versatility.[22,23] These low-dimensional materials are also investigated for their potential use in technological applications.[24–26] Predictive computational modeling of related low-dimensional systems at comparable levels of theory has provided reliable descriptions of their structural, electronic, and optical properties, in several cases corroborated by experiment.[27,28] They can be synthesized through different methods and exhibit structural, mechanical, and electronic properties that can be modulated, which is essential for the development of advanced nanotechnologies.[21,29–33] The literature also reports several graphene inorganic analogues that can form nanoscrolls, including borophene,[34] molybdenum disulfide (MoS_2),[33,35] and tungsten diselenide (WSe_2),[36] among others.[37–39]

Among different two-dimensional materials, cobalt oxides have attracted particular interest due to their electronic structure, high surface area, and suitability for redox reactions. Although metastable in their monolayer form, they exhibit a ferromagnetic ground state and a metallic band structure, combined with strong electron–phonon coupling, which can give rise to phonon-mediated superconductivity at temperatures between 25 and 28 K.[40–43] More recently, Hettler *et al.* synthesized CoO_2 nanoscrolls, demonstrating that the scrolled morphology can stabilize these metastable materials.[44] Additional studies have reported remarkable electronic properties for these systems. These findings underscore the need for a more detailed theoretical investigation to provide deeper insight into the structural and electronic behavior of CoO_2 nanoscrolls and to assess their thermal stability.

In this work, we have investigated CoO_2 nanoscrolls through Density Functional Tight-Binding (DFTB) simulations, focusing on their structural and electronic characteristics as well as their thermal stability. Different scroll geometries were considered to examine factors that influence stability and charge distribution. The study establishes a theoretical description that complements

[a] Applied Physics Department and Center for Computational Engineering & Sciences, State University of Campinas, Campinas, São Paulo, 13083-970, Brazil. E-mail: galvao@ifi.unicamp.br
[b] Physics Department, São Paulo State University (UNESP), 13506-900, Rio Claro, SP, Brazil
[c] University of Brasília, College of Technology, Department of Electrical Engineering, Brasília, Federal District, 70910-900, Brazil

recent experimental advances and contributes to a deeper understanding of transition-metal oxide nanoscrolls as emerging low-dimensional systems.

2 Computational details

The CoO_2 nanoscrolls (Fig. 1) were generated from rectangular monolayers passivated by O_2 at the outer edge and Co at the inner edge. The creation of these structural models can be described in polar coordinates as $r\ (\theta) = a + b\theta$, where a corresponds to the internal scroll radius and b is related to the interlayer scroll spacing. In this work, we adopted $a = 10$ Å and $b = 4$ Å. Three different scroll structures were considered by taking $\theta = 540^\circ$ (1.5 turns), $\theta = 720^\circ$ (2 turns), and $\theta = 1080^\circ$ (3 turns). We carried out full geometry optimizations of the layers prior to the rolling process.

Geometry optimizations were performed with the Rational algorithm under self-consistent charge conditions, adopting convergence thresholds of 10^{-8} for total energy, 10^{-7} Ha for the SCC cycle, and 0.05 eV Å^{-1} for the force gradient.

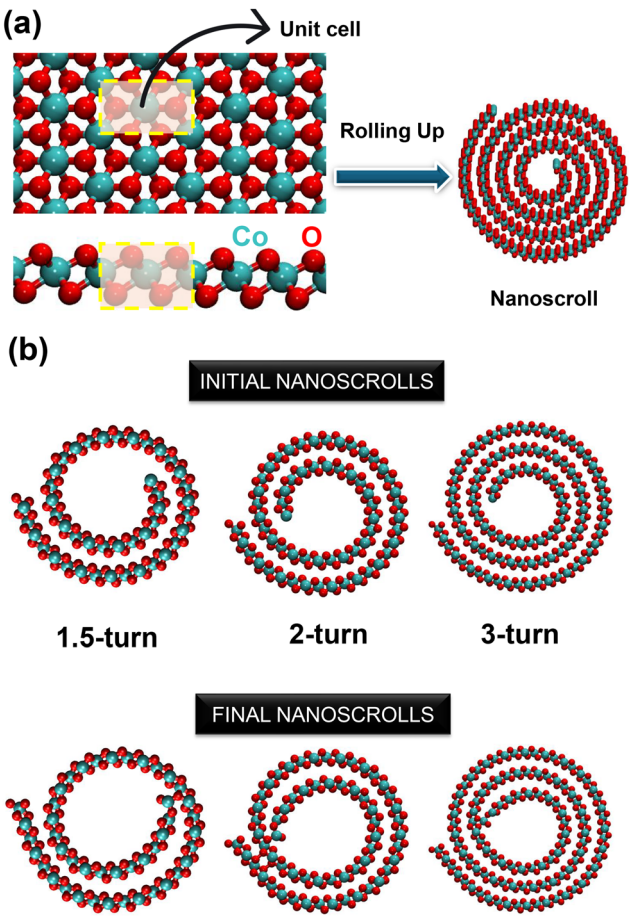

Fig. 1 (a) Representation of the CoO_2 monolayer and the scheme of the rolling process that leads to the formation of nanoscrolls. The highlighted unit cell is shown from the top and side views, with cobalt and oxygen atoms indicated. (b) Initial configurations of CoO_2 nanoscrolls with 1.5, 2, and 3 turns and their final geometries after full structural optimization. Cobalt and oxygen atoms are shown in blue and red, respectively.

Molecular dynamics simulations were carried out over the temperature range from 10 K to 600 K in the NVT ensemble, using the Verlet integration algorithm and a Nosé-Hoover thermostat. A timestep of 1 fs and approximately 10 000 steps were used, with the constant-temperature plateau being reached within about 1 ps and maintained throughout the remainder of the run. The systems were subsequently heated to 600 K during 1000 steps and re-equilibrated.

All simulations were carried out within the self-consistent charge Density Functional Tight-Binding (SCC-DFTB) approximation using the DFTB+ code,[45,46] which enables the evaluation of structural relaxation, electronic properties, and molecular dynamics runs at relatively (in comparison to full DFT methods) low computational cost while maintaining accuracy comparable to that of some density functional theory approaches.

Within the standard DFTB framework, the Hamiltonian is constructed considering only two-center contributions. Since these terms decay rapidly with increasing interatomic separation, they do not adequately describe long range interactions such as van der Waals forces. To overcome this limitation, a dispersion correction is introduced through a Lennard-Jones type potential as proposed by Zhechkov *et al.*[47] For interatomic distances larger than the cutoff radius r_0, the interaction potential is given by

$$U_{ij}(r) = d_{ij}\left[-2\left(\frac{r_{ij}}{r}\right)^6 + \left(\frac{r_{ij}}{r}\right)^{12}\right]. \quad (1)$$

This expression describes the attractive regime of the interaction. For short interatomic distances, a repulsive polynomial form is adopted. In this regime, defined by $r < r_0$, the potential is written as

$$U_{ij}\,(r) = U_0 - U_1 r^5 - U_2 r^{10}. \quad (2)$$

The transition between the attractive and repulsive regimes is determined by the cutoff radius r_0. The coefficients entering the repulsive potential follow the definitions introduced in ref.[47] and are given by

$$U_0 = \frac{396}{25} d_{ij}, \quad (3)$$

$$U_1 = 2^{5/6}\frac{672}{25}\frac{d_{ij}}{r_{ij}^5}, \quad (4)$$

$$U_2 = -2^{2/3}\frac{552}{25}\frac{d_{ij}}{r_{ij}^{10}}. \quad (5)$$

The parameters r_{ij}, corresponding to the van der Waals distance, and d_{ij}, corresponding to the potential well depth, are taken from the parametrization reported by Zhechkov *et al.*[47] and from the Universal Force Field framework.[48] These parameters are distributed together with the DFTB+ implementation.[46] In order to ensure the reliability of our methodology, DFTB description was benchmarked against available literature data for CoO_2, including reported experimental interlayer spacing and previously published theoretical/experimental structural parameters.

3 Results and discussion

As previously described, the nanoscroll structures were generated by rolling up rectangular supercells of the CoO_2 monolayer using a model developed and applied in our earlier work,[34] followed by structural optimizations performed with DFTB+. For the CoO_2 monolayer, the results indicate a monoclinic $C1m1$ space group consisting of six atoms in the unit cell, with lattice parameters $a = 4.724$ Å, $b = 2.768$ Å, and $\beta = 98.1505^\circ$. The Co-O bond lengths range from 1.82 Å to 1.84 Å, while the Co-Co distance is 2.66 Å. These values are in good agreement with those reported in the literature based on DFT calculations and experimental measurements.[49]

Subsequently, three nanoscrolls were constructed with 1.5, 2, and 3 turns, exhibiting an initial interlayer spacing (d) of 4 Å and an initial internal radius (r) of 10 Å. In the rolling process, three rectangular supercells were employed with dimensions of 2.61 Å × 93.76 Å, 2.61 Å × 140.99 Å, and 2.61 Å × 251.92 Å, corresponding to the 1.5-, 2-, and 3-turn nanoscrolls, respectively (see Fig. 1). In all cases, the periodic simulation cell was defined to preserve periodicity along the rolling axis and to avoid interactions between virtual replicas of the system, with 100 Å in the non-periodic directions. The unit cells of the 1.5-, 2-, and 3-turn CoO_2 nanoscrolls contain 129, 180, and 321 atoms, respectively, and their structures were designed to preserve the known stoichiometry. Using the spiral construction parameters adopted in this work, the 1.5-, 2-, and 3-turn nanoscrolls have external diameters of approximately 3.2, 3.6, and 4.4 nm and an internal radius of about 1 nm. The periodicity along the rolling axis effectively represents infinite scrolls, so the models correspond to local cross sections of the much larger nanoscrolls (external diameters of 120–200 nm and wall thicknesses of about 5 nm) reported in the experimental synthesis.[44]

After the structural optimization of the nanoscrolls, we observed that the average interlayer spacing remained approximately 0.46 nm, regardless of the number of turns. This value, which is significantly larger than that found for carbon nanoscrolls ($\sim$0.35 nm),[50] closely matches the experimentally reported value of 0.44 nm,[44] with a deviation of only 4.5%. The calculated Co–O and Co–Co bond lengths were 1.90 Å and 2.71 Å, respectively, differing by approximately 4.4% and 1.9% from those found in the monolayer structure. The modest bond-length deviations relative to the planar monolayer (about 4% for Co–O and 2% for Co–Co) are consistent with the small per-atom scrolling energy and indicate that the curvature is accommodated mainly by changes in bond orientation rather than by bond stretching, so that the local octahedral coordination of Co is preserved upon rolling.

To analyze the stability of the systems investigated here, we calculated the scrolling energy (E_{sc}) using the expression $E_{sc} = E_{scroll} - E_{strip}$, where E_{scroll} and E_{strip} correspond to the total energies of the nanoscroll and the respective planar nanostrip. The results indicate that nanoscrolls with 1.5 turns or more present negative E_{sc} values compared to their two-dimensional counterparts, with thermodynamic stability increasing as the number of turns increases (−0.01, −0.06, and −0.10 eV per atom for the 1.5-, 2-, and 3-turn configurations, respectively). Although none of the rolled configurations exhibits a lower total energy per atom than the infinite CoO_2 surface, which is itself considered a metastable phase, the nanoscrolls can be regarded as structurally stable arrangements. The stabilization mechanism for CoO_2 nanoscrolls can be understood as a result of two competing energetic contributions, namely the increase in elastic energy due to bending and the van der Waals energy decrease caused by the approximation of subsequent layers during the rolling process.

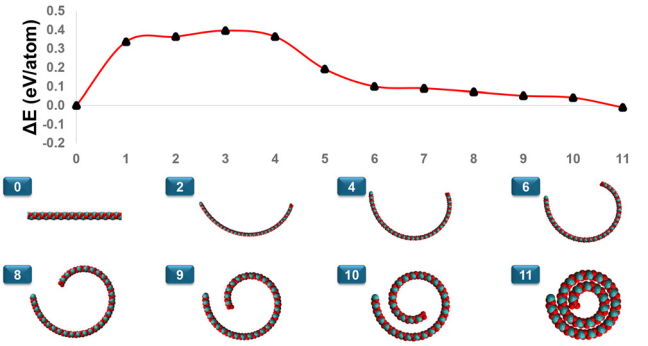

Fig. 2 Relative energy stability values in the CoO_2 nanoscroll rolling process and their corresponding structural configurations.

To further understand the formation process of these systems, Fig. 2 illustrates the relative stability profile throughout the rolling process. As the structure begins to bend, the energy cost initially increases due to mechanical strain until a critical point is reached, at which dispersion forces become dominant and lead to a net stabilization of the system. This behavior is consistent with previous reports on carbon nanoscrolls[51] and borophene nanoscrolls,[34] in which the rolling mechanism is also governed by the interplay between bending rigidity and attractive van der Waals forces. Furthermore, while isolated planar nanostrips are not experimentally observed after synthesis, nanoscrolls are consistently observed, indicating that the scrolled configuration is favored under realistic thermodynamic and kinetic conditions. This agreement between theoretical predictions and experimental findings reinforces the reliability of our computational framework. It supports the physical plausibility of the metastable two-dimensional structures when transformed into the quasi-one-dimensional systems proposed here.

Molecular dynamics simulations further demonstrated that the CoO_2 nanoscrolls are highly stable, withstanding temperatures up to 600 K without fracture or unscrolling. However, the degree of structural distortion increases as the number of turns decreases. Quantitatively, for the two-turn nanoscroll under a 100–300 K thermal ramp followed by a 300 K plateau (5 ps each), the spiral topology is preserved throughout the run, with no fracture or unrolling. The local interlayer distance distribution at 300 K is bimodal, with a dominant stacked population at $\langle d_{int}^{local} \rangle$ = 0.458 nm (73%), in agreement with the relaxed value of 0.46 nm and the experimental spacing of 0.44 nm, and a secondary expanded-interlayer population centered at 0.72 nm (27%) localized in angular sectors adjacent to the open outer edge of the

spiral. The plateau-averaged value of 0.515 nm is therefore not a homogeneous thermal expansion but reflects this minority expanded-interlayer fraction arising from the open-ended geometry of the simulation cell. The local interlayer spacing remains essentially uniform along the body of the scroll, where the relaxed value is preserved, while the expanded-interlayer fraction arises from the kinematic constraint imposed by the Co–O–Co bridge that anchors the outer edges to the previous winding layer and prevents the spiral from gliding freely under thermal motion, confining the local relaxation to the scrolled regions adjacent to the open outer edge.

Regarding the electronic structure, Fig. 3(a), 4(a), and 5(a) indicate that the major contribution for the density of states near the Fermi level is due to cobalt d-orbitals, followed by oxygen p-orbitals, with all other contributions negligibly small. Since these orbitals remain partially occupied even after bending, the metallic character is preserved for the scrolled structures. It is interesting to note that, despite the significant deformation, the electronic structure modifications were modest, with no signs of flat bands near the Fermi level or even of Dirac-like features. Fig. 3(b), 4(b), and 5(b) present the charge differences for the CoO_2 nanoscrolls with 1.5, 2, and 3 turns. In all cases, oxygen atoms play the dominant role in charge displacement. Oxygen atoms accumulate charge while a depletion is observed for cobalt. This charge transfer can lead to polarization effects that should be investigated in the near future.

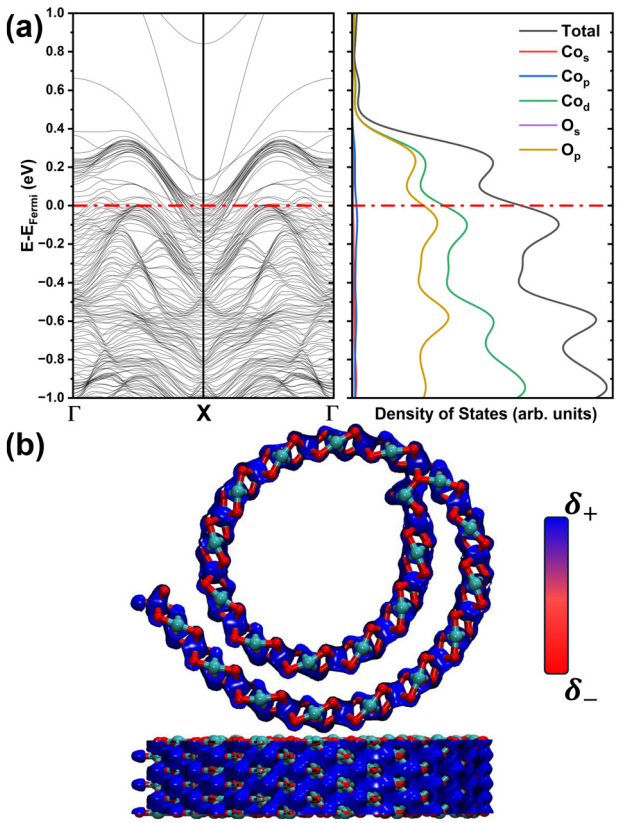

Fig. 3 (a) Electronic band structure and the corresponding projected density of states of the 1.5-turn CoO_2 nanoscroll. (b) Charge density difference showing regions of accumulation (δ_+) and charge depletion (δ_-).

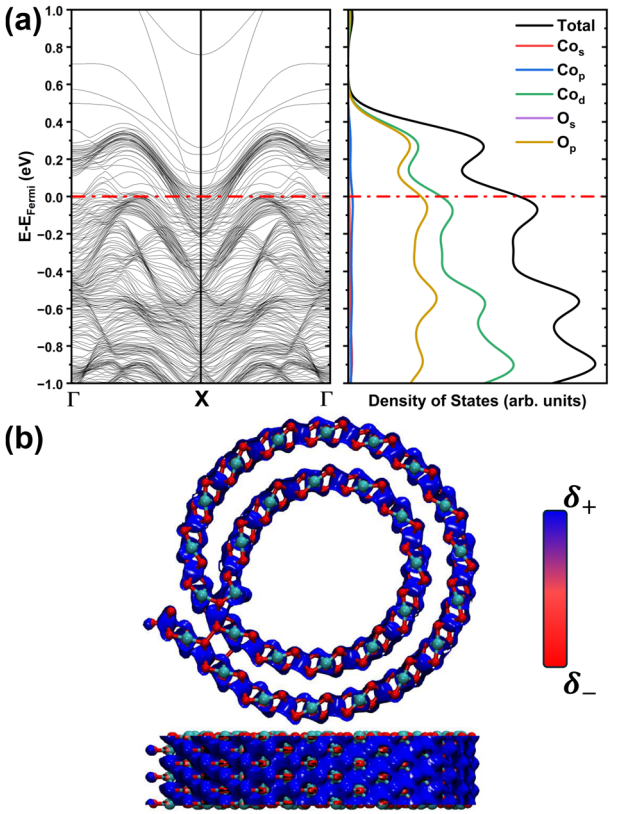

Fig. 4 (a) Electronic band structure and the corresponding projected density of states of the 2-turn CoO_2 nanoscroll. (b) Charge density difference showing regions of accumulation (δ_+) and charge depletion (δ_-).

Mulliken population analysis of the optimized two-turn nanoscroll yields mean atomic charges of $+0.56 \pm 0.11e$ on Co and $-0.28 \pm 0.03e$ on O, quantitatively confirming the Co → O polarization suggested by the charge density difference. Partitioning the atoms into the inner and outer walls of the scroll reveals a slight enhancement of the polarization on the outer wall, with $\langle q_{Co}\rangle_{outer} = +0.57e$ *versus* $\langle q_{Co}\rangle_{inner} = +0.54e$ and $\langle q_O\rangle_{outer} = -0.29e$ *versus* $\langle q_O\rangle_{inner} = -0.27e$. One Co atom located at the free outer edge of the scroll carries an anomalously large charge of $+1.16e$, consistent with its undercoordinated environment at the open edge. This site forms unusually short Co–O bonds with the passivating oxygens of the outer edge (1.63 and 1.70 Å against 1.78–1.91 Å at the bulk-like sites of the scroll), while two further oxygens of its coordination shell bridge to the adjacent cobalt of the same outermost turn through Co–O–Co linkages of standard length, anchoring the terminator to the underlying winding. The associated local polarization drains charge from the cobalt atoms at the edges and spatially coincides with the LUCO localization pattern reported in Fig. 6, identifying the open outer edge as a natural candidate for preferential adsorption. The systems considered here are pristine; defect states such as oxygen vacancies or Co substitutions would be expected to locally modify the interlayer spacing and to introduce features close to the Fermi level, weakening in particular the Co–O polarization quantified above. A systematic defect study lies outside the scope of the present work and constitutes a natural

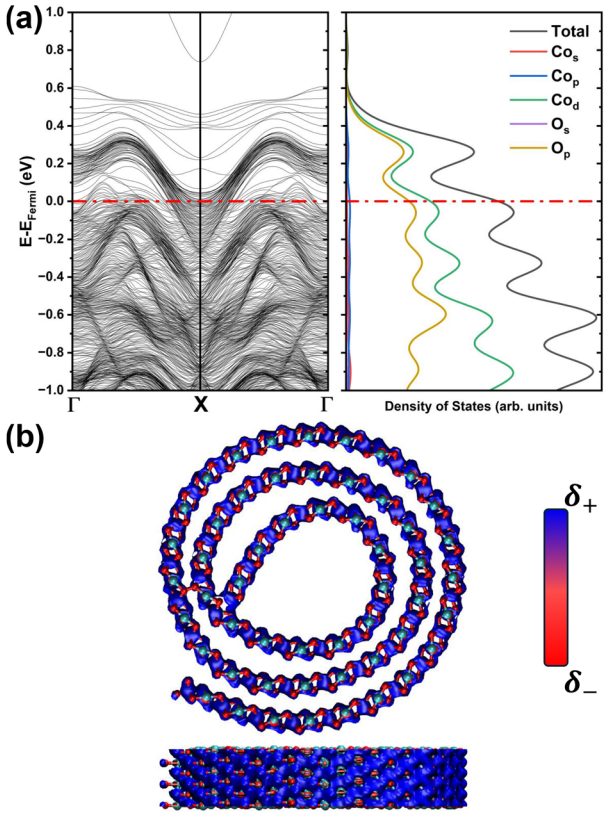

Fig. 5 (a) Electronic band structure and the corresponding projected density of states of the 3-turn CoO_2 nanoscroll. (b) Charge density difference showing regions of accumulation (δ_+) and charge depletion (δ_-).

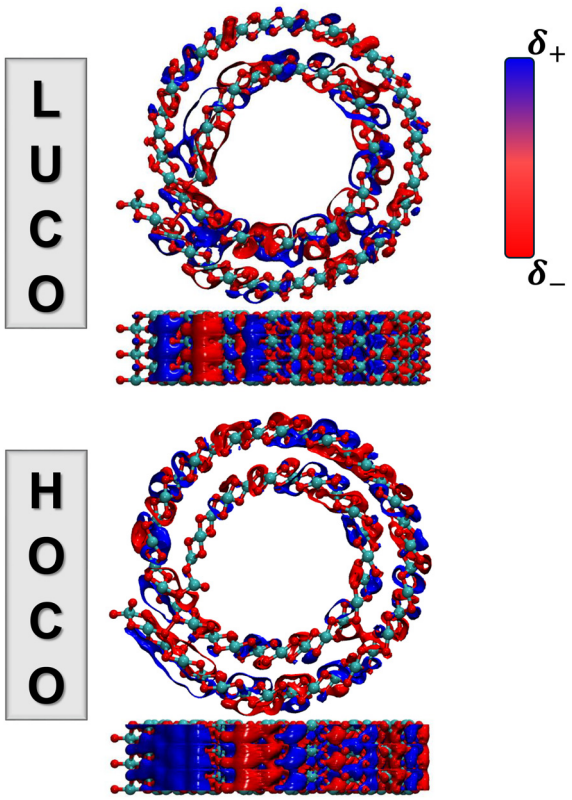

Fig. 6 Lowest Unoccupied Crystal Orbital (LUCO) and Highest Occupied Crystal Orbital (HOCO) of 2-turn CoO_2 nanoscrolls.

follow-up. In addition to the charge difference, the HOCO and LUCO were also calculated to provide a deeper understanding of the electronic modifications induced by the rolling process. The results are shown in Fig. 6. The HOCO exhibits significant accumulation at the inner edge, where bonding to the nanoscroll's internal wall begins, with a higher orbital density in this region.

In contrast, the outer edge exhibits a low HOCO density. The LUCO reveals the opposite HOCO trend, with a decrease of orbital density at the inner edge and a substantial increase at the outer one. Both the HOCO and LUCO display homogeneous regions except at the inner and outer edges.

4 Conclusions

In conclusion, the results presented in this work provide, for the first time, a comprehensive theoretical perspective on the structural and electronic properties of CoO_2 nanoscrolls, identifying the intrinsic metallic character of these nanostructures regardless of the winding orientation or the number of turns. Oxygen atoms are shown to play a central role in mediating charge transfer processes, with pronounced electronic interactions occurring between the inner edge of the scroll and the adjacent layers. From a structural standpoint, it is noteworthy that the scroll topology creates a metastability of CoO_2 in its two-dimensional form while preserving its intrinsic structural and electronic characteristics. The results presented here are in agreement with recent experimental synthesis reports, reinforcing the robustness and reliability of the computational approach adopted.

Author contributions

Guilherme S. L. Fabris: data curation, software, formal analysis, investigation, visualization, and writing – original draft. Ricardo Paupitz: conceptualization, formal analysis, supervision, funding acquisition, validation, investigation, methodology, and writing – review & editing. Marcelo L. Pereira Junior: resources, software, formal analysis, supervision, funding acquisition, validation, investigation, methodology, and writing – review & editing. Douglas S. Galvão: conceptualization, resources, formal analysis, supervision, funding acquisition, validation, investigation, project administration, and writing – review & editing.

Conflicts of interest

There are no conflicts to declare.

Data availability

The data that support the findings of this study are available from the corresponding author upon reasonable request.

Acknowledgements

Guilherme S. L. Fabris acknowledges the São Paulo Research Foundation (FAPESP) fellowship (process number #2024/03413-9). Ricardo Paupitz acknowledges CNPq for grant #313592/2023-3. Marcelo L. Pereira Junior acknowledges financial support from FAPDF (grant 00193-00001807/2023-16), CNPq (grants 444921/2024-9 and 308222/2025-3), and CAPES (grant 88887.005164/2024-00). Douglas S. Galvão acknowledges the Center for Computing in Engineering and Sciences at Unicamp for financial support through the FAPESP/CEPID Grant (process number #2013/08293-7). We thank the Coaraci Supercomputer for computer time (FAPESP grant #2019/17874-0). DSG also acknowledges support from INEO/CNPQ and FAPESP grant 2025/27044-5.

References

1 Q. Tang and Z. Zhou, *Prog. Mater. Sci.*, 2013, **58**, 1244–1315.
2 M. Dresselhaus, *Mater. Res. Lett.*, 2014, **2**, 1–9.
3 Paras, K. Yadav, P. Kumar, D. R. Teja, S. Chakraborty, M. Chakraborty, S. S. Mohapatra, A. Sahoo, M. M. Chou and C.-T. Liang, *et al.*, *Nanomaterials*, 2023, **13**, 160.
4 A. K. Geim and K. S. Novoselov, *Nat. Mater.*, 2007, **6**, 183–191.
5 P. Vogt, P. De Padova, C. Quaresima, J. Avila, E. Frantzeskakis, M. C. Asensio, A. Resta, B. Ealet and G. Le Lay, *Phys. Rev. Lett.*, 2012, **108**, 155501.
6 Y. Liu, L. Wu and L. He, *Phys. Chem. Chem. Phys.*, 2025, **27**, 14100–14112.
7 J. Ji, X. Song, J. Liu, Z. Yan, C. Huo, S. Zhang, M. Su, L. Liao, W. Wang, Z. Ni, Y. Hao and H. Zeng, *Nat. Commun.*, 2016, **7**, 13352.
8 M. Xie, S. Zhang, B. Cai, Y. Gu, X. Liu, E. Kan and H. Zeng, *Nano Energy*, 2017, **38**, 561–568.
9 D. Golberg, Y. Bando, Y. Huang, T. Terao, M. Mitome, C. Tang and C. Zhi, *ACS Nano*, 2010, **4**, 2979–2993.
10 S. Guo, Y. Zhang, Y. Ge, S. Zhang, H. Zeng and H. Zhang, *Adv. Mater.*, 2019, **31**, 1902352.
11 S. Zhang, S. Guo, Z. Chen, Y. Wang, H. Gao, J. Gómez-Herrero, P. Ares, F. Zamora, Z. Zhu and H. Zeng, *Chem. Soc. Rev.*, 2018, **47**, 982–1021.
12 S. Kulkarni Vishakha, D. Butte Kishor and S. Rathod Sudha, *Int. J. Res. Pharm. Biomed. Sci.*, 2012, **3**, 1597–1613.
13 A. K. Mohanty, F. Wu, R. Mincheva, M. Hakkarainen, J.-M. Raquez, D. F. Mielewski, R. Narayan, A. N. Netravali and M. Misra, *Nat. Rev. Methods Primers*, 2022, **2**, 46.
14 S. Dutta and S. K. Pati, *J. Mater. Chem.*, 2010, **20**, 8207–8223.
15 S. Lou, B. Lyu, X. Zhou, P. Shen, J. Chen and Z. Shi, *Quantum Front.*, 2024, **3**, 3.
16 R. Maheswaran and B. P. Shanmugavel, *J. Electron. Mater.*, 2022, **51**, 2786–2800.
17 C. N. R. Rao, B. Satishkumar, A. Govindaraj and M. Nath, *Chem. Phys. Chem.*, 2001, **2**, 78–105.
18 X. Shi, N. M. Pugno and H. Gao, *Acta Mech. Solida Sin.*, 2010, **23**, 484–497.
19 E. Perim, L. D. Machado and D. S. Galvao, *Front. Mater.*, 2014, **1**, 31.
20 S. Aftab, M. Z. Iqbal and Y. S. Rim, *Small*, 2023, **19**, 2205418.
21 G. Mpourmpakis, E. Tylianakis and G. E. Froudakis, *Nano Lett.*, 2007, **7**, 1893–1897.
22 E. Perim, R. Paupitz and D. S. Galvao, *J. Appl. Phys.*, 2013, **113**, 054306.
23 R. Rurali, V. R. Coluci and D. S. Galvão, *Phys. Rev. B:Condens. Matter Mater. Phys.*, 2006, **74**, 085414.
24 X. Peng, *Adsorption*, 2024, **30**, 1937–1946.
25 Y. Gao, M. Maruyama and S. Okada, *Jpn. J. Appl. Phys.*, 2024, **63**, 085001.
26 H. Luo, X. Zhang, H. Zhu, K. Zhang, F. Yang, K. Xu, S. Yu and D. Guo, *J. Mater. Sci. Technol.*, 2023, **166**, 164–172.
27 R. R. Pela, C.-L. Hsiao, L. Hultman, J. Birch and G. K. Gueorguiev, *Phys. Chem. Chem. Phys.*, 2024, **26**, 7504–7514.
28 G.-Q. Mao, Z.-Y. Yan, K.-H. Xue, Z. Ai, S. Yang, H. Cui, J.-H. Yuan, T.-L. Ren and X. Miao, *J. Phys.: Condens. Matter*, 2022, **34**, 403001.
29 H.-q Zhou, C.-y Qiu, H.-c Yang, F. Yu, M.-j Chen, L.-j Hu, Y.-j Guo and L.-f Sun, *Chem. Phys. Lett.*, 2011, **501**, 475–479.
30 D. Xia, Q. Xue, J. Xie, H. Chen, C. Lv, F. Besenbacher and M. Dong, *Small*, 2010, **6**, 2010–2019.
31 X. Shi, N. M. Pugno and H. Gao, *J. Comput. Theor. Nanosci.*, 2010, **7**, 517–521.
32 X. Shi, Y. Cheng, N. M. Pugno and H. Gao, *Small*, 2010, **6**, 739–744.
33 Z. Wang, H.-H. Wu, Q. Li, F. Besenbacher, X. C. Zeng and M. Dong, *Nanoscale*, 2018, **10**, 18178–18185.
34 G. S. Fabris, D. S. Galvão and R. Paupitz, *Phys. Chem. Chem. Phys.*, 2024, **26**, 11589–11596.
35 S. Qiao, Y. Qiu, Y. Lu, Z. Wang, M. Yuan and Q. Ji, *Nano Lett.*, 2024, **24**, 4498–4504.
36 Z. Ao, C. Liu, H. Ma, X. Lan, J. Zhang, B. Zhang, F. Zhang, Z. Wang, P. Chen, M. Zhong, G. Wang and Z. Zhang, *Small*, 2024, **20**, 2404897.
37 J.-H. Kim and T.-M. Lu, *RSC Adv.*, 2016, **6**, 17179–17187.
38 A. D. Sontakke and M. K. Purkait, *Chem. Eng. J.*, 2021, **420**, 129914.
39 M. Kaneda, W. Zhang, Z. Liu, Y. Gao, M. Maruyama, Y. Nakanishi, H. Nakajo, S. Aoki, K. Honda, T. Ogawa, K. Hashimoto, T. Endo, K. Aso, T. Chen, Y. Oshima, Y. Yamada-Takamura, Y. Takahashi, S. Okada, T. Kato and Y. Miyata, *ACS Nano*, 2024, **18**, 2772–2781.
40 D. Nguyen, C. Hsing and C.-M. Wei, *Nanoscale*, 2019, **11**, 17052–17057.
41 M. Pu, Y. Guo and W. Guo, *Nanoscale Horiz.*, 2022, **7**, 1404–1410.
42 C. C. Leong, H. Pan and S. Ho, *Phys. Chem. Chem. Phys.*, 2016, **18**(10), 7527–7534.
43 X.-L. Xu, C.-E. Hu, H.-J. Wu, H. Geng and X. Chen, *J. Appl. Phys.*, 2024, **135**, 214301.
44 S. Hettler, K. S. Roy, R. Arenal and L. S. Panchakarla, *Adv. Mater. Interfaces*, 2024, **11**, 2400317.
45 M. Elstner, D. Porezag, G. Jungnickel, J. Elsner, M. Haugk, T. Frauenheim, S. Suhai and G. Seifert, *Phys. Rev. B:Condens. Matter Mater. Phys.*, 1998, **58**, 7260–7268.
46 B. Hourahine, B. Aradi, V. Blum, F. Bonafé, A. Buccheri, C. Camacho, C. Cevallos, M. Y. Deshaye, T. Dumitrică,

A. Dominguez, S. Ehlert, M. Elstner, T. van der Heide, J. Hermann, S. Irle, J. J. Kranz, C. Kohler, T. Kowalczyk, T. Kubař, I. S. Lee, V. Lutsker, R. J. Maurer, S. K. Min, I. Mitchell, C. Negre, T. A. Niehaus, A. M. N. Niklasson, A. J. Page, A. Pecchia, G. Penazzi, M. P. Persson, J. Řezáč, C. G. Sanchez, M. Sternberg, M. Stöhr, F. Stuckenberg, A. Tkatchenko, V. W. Z. Yu and T. Frauenheim, *J. Chem. Phys.*, 2020, **152**, 124101.

47 L. Zhechkov, T. Heine, S. Patchkovskii, G. Seifert and H. A. Duarte, *J. Chem. Theory Comput.*, 2005, **1**, 841–847.

48 A. K. Rappe, C. J. Casewit, K. S. Colwell, W. A. Goddard and W. M. Skiff, *J. Am. Chem. Soc.*, 1992, **114**, 10024–10035.

49 P. Ferstl, F. Mittendorfer, J. Redinger, M. A. Schneider and L. Hammer, *Phys. Rev. B*, 2017, **96**, 085407.

50 X. Xie, L. Ju, X. Feng, Y. Sun, R. Zhou, K. Liu, S. Fan, Q. Li and K. Jiang, *Nano Lett.*, 2009, **9**, 2565–2570.

51 S. F. Braga, V. R. Coluci, S. B. Legoas, R. Giro, D. S. Galvao and R. H. Baughman, *Nano Lett.*, 2004, **4**, 881–884.